EXPERIMENTAL VALIDATION OF A MODEL OF AN UNCONTROLLED BICYCLE

A. L. Schwab[ℵ], J. P. Meijaard[*], and J. D. G. Kooijman[ℵ]

[ℵ]Delft University of Technology
Laboratory for Engineering Mechanics
Mekelweg 2, NL-2628 CD Delft, The Netherlands
a.l.schwab@tudelft.nl

[*] School of MMME
The University of Nottingham, Nottingham, UK

Keywords: Bicycle dynamics, experiments, instrumentation, multibody dynamics.

Abstract. *In this paper, an experimental validation of some modelling aspects of an uncontrolled bicycle is presented. In computer models, many physical aspects of the real bicycle are considered negligible, such as the flexibility of the frame and wheels, play in the bearings, and precise tire characteristics. The admissibility of these assumptions has been checked by comparing experimental results with numerical simulation results.*

The numerical simulations were performed on a benchmarked bicycle model. This model consisted of four rigid bodies connected by revolute joints. The contact between the knife-edge wheels and the flat level surface was modelled by holonomic constraints in the normal direction and by non-holonomic constraints in the longitudinal and lateral direction. In the absence of a rider we assumed no-hands operation. For the validation we considered the linearized equations of motion for small perturbations of the upright steady forward motion. Apart from flexibility and play, the greatest uncertainty that was verified in this model was the replacement of the tires by ideal rolling knife-edge wheels.

The experimental system consisted of an instrumented bicycle without rider. Sensors were present for measuring the roll rate and the yaw rate, the steering angle and the rear wheel rotation. Trainer wheels prevented the complete fall of the bicycle for unstable conditions.

Measurements were recorded for the case in which the bicycle coasted freely on a level surface. From these measured data eigenvalues were extracted by means of curve fitting. These eigenvalues were then compared with the results from the linearized equations of motion of the model. As a result, the model appeared to be fairly accurate for the low-speed low-frequency behaviour.
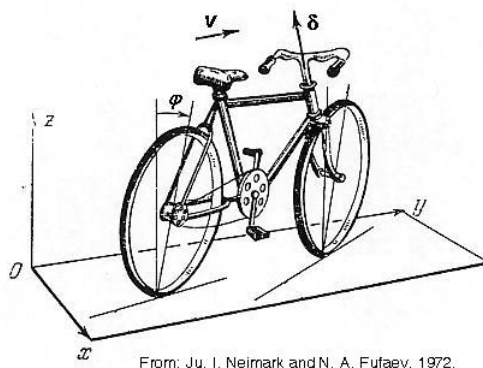
From: Ju. I. Neimark and N. A. Fufaev, 1972.

Figure 1: The bicycle model: four rigid bodies (rear wheel, rear frame plus rigid rider, front handlebar assembly, front wheel) connected by three revolute joints (rear hub, steering axis, front hub).

1 Introduction

Everybody knows that a bicycle is highly unstable at low speeds whereas it is easy to stabilize at moderate to high speeds. This speed dependant stability is already present in one of the simplest bicycle models, consisting of four rigid bodies connected by three revolute joints, figure 1. In this model the rider is rigidly attached to the frame and his hands are free from the handlebar. For the knife edge wheels we assume pure rolling contact, and no side slip. The resulting non-holonomic mechanical model has three velocity degrees of freedom: forward speed v, lean rate $\dot{\phi}$ and steering rate $\dot{\delta}$. Starting from an upright steady motion this uncontrolled model can show, after perturbing laterally, asymptotically stable motion in a certain speed range, despite the fact that the model is energy conservative.

The governing dynamic equations for this model have recently been benchmarked [1] and after more than a century of bicycle dynamics literature we are now certain that these equations are correct. In this model, many physical aspects of the real bicycle are considered negligible, such as the flexibility of the frame and wheels, play in the bearings, and precise tire characteristics. The admissibility of these assumptions is checked by comparing experimental results with numerical simulation results. Apart from flexibility and play, the greatest uncertainty to be verified in this model is the replacement of the tires by ideal rolling knife-edge wheels.

The experimental system consists of an instrumented bicycle without rider. Sensors are present for measuring the roll rate and the yaw rate, the steering angle and the rear wheel rotation. Trainer wheels prevent the complete fall of the bicycle for unstable conditions. Measurements are recorded for the case in which the bicycle, after being manually pushed off, coasts freely on a level surface. From these measured data eigenvalues are extracted by means of curve fitting. These eigenvalues are then compared with the results from the linearized equations of motion of the model.

The literature on experimental verification of modelling aspects in single-track vehicles can be divided in two sections: bicycles and motorcycles. We know from experience that tires play a dominant role in the dynamic behaviour of a motorcycle at high speed. Since the model under study here operates at low speed and assumes ideal rolling contact, it seems that many motorcycle studies lie outside the current scope. Döhring [2, 3] was the first to measure the lateral motion of a single track vehicle. Although he measured on three motorcycles he compared his results with the same model as presented here and this can therefore be classified as bicycle dynamics. Rice and Roland [4] measured the lateral stability and control of two distinct bicycles, both in hands-free as well as controlled operation. Roland and Lynch [5] performed an exten-
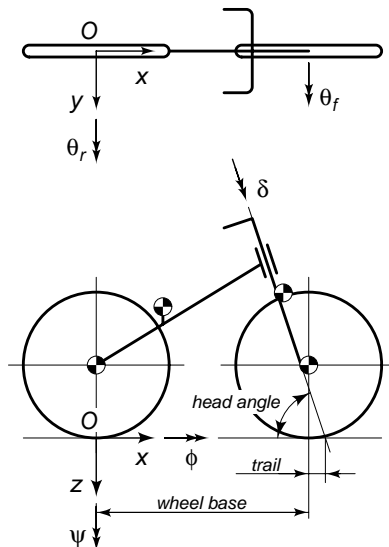
Figure 2: Bicycle model together with the coordinate system, the degrees of freedom, and the parameters.

sive study in lateral bicycle dynamics. They measured tire characteristics and then performed a number of tests on an instrumented uncontrolled bicycle and compared the results with their model (Roland and Massing [6]). Wächter [7] and Suhr [8] performed some experimental validation for their bicycle dynamics model. Jackson and Dragovan [9] measured the state of a bicycle ridden hands-free and compared the time history with results from their model.

Many measurement have been made on the lateral dynamics of motorcycles. We discuss here only some distinct contributions. Eaton [10] measured the transient response of a light motorcycle to a lateral disturbance and compared this with his model. Rice [11] performed a number of tests on motorcycles in order to obtain performance characteristics for handling and safety. Weir and Zellner [12] tested transient behaviour of motorcycles in some standard manoeuvrers and compared some results with their model. Ruijs and Pacejka [13] built a rider robot to validate their computer model eliminating disturbances originating from the human rider. Rider robots have also been built by the group of Kageyama [14] and the Blue Team [15], a group of Berkeley students engaged in the DARPA challenge. Cossalter, Doria and Lot [16] over the past decade performed an extensive range of measurement on several aspects of the dynamic behaviour of motorcycles.

2 BICYCLE MODEL

The mechanical model of the bicycle is described in [1] and consists of four rigid bodies, viz. the rear frame, the front frame being the front fork and handlebar assembly and the two knife-edge wheels. The bodies are interconnected by revolute hinges at the steering head between the rear frame and the front frame and at the two wheel hubs. In the reference configuration, all bodies are assumed to be symmetric relative to the bicycle midplane. The contact between the wheels and the flat level surface is modelled as stiff and non-slipping by holonomic constraints in the normal direction and by non-holonomic constraints in the longitudinal and lateral direction. It is assumed that there is no friction, apart from the idealized friction between the non-slipping wheels and the surface, and no propulsion. These assumptions make the model energy-conserving. In the reference position, the global Cartesian coordinate system is located at the rear wheel contact point O, where the x-axis points in the longitudinal direction of the

bicycle and the z-axis is directed downwards. Figure 2 shows the directions of the axes.

The mechanical model of the bicycle has three velocity degrees of freedom: the roll rate $\dot{\phi}$ of the rear frame, the steering rate $\dot{\delta}$, and the angular rate $\dot{\theta}_r$ of the rear wheel with respect to the rear frame. The dimensions and mechanical properties of the instrumented bicycle are presented on page 12 in table 1. The instrumented bicycle is assumed symmetric about the vertical longitudinal plane and the wheels are assumed rotationally symmetric about their axles. The mass moments of inertia are given with respect to axis through the centre of mass and parallel to the global xyz-axes in the reference position.

The governing equations of motion represent a linear perturbation of a constant-speed straight-ahead upright solution: $\phi = 0$, $\delta = 0$, and the constant forward speed is $v = -\dot{\theta}_r R_{rw}$.

The lateral symmetry of the system, combined with the linearity in the equations precludes any coupling between the forward motion and the lean and steer. For example, a lean to the right must cause the same speed-up as a lean to the left. But linearity requires the effects to be the opposite of each other. Thus there can be no linear coupling. Therefore the first linearized equation of motion is

$$\ddot{\theta}_r = 0. \tag{1}$$

Consequently the nominal forward speed $v = -\dot{\theta}_r R_{rw}$ is constant.

The linearized equations of motion for the bicycle expressed in the two remaining degrees of freedom, the lean angle ϕ and the steer angle δ, are two coupled second-order constant-coefficient ordinary differential equations with the forward speed as a parameter. The first equation is called *the lean equation* and the second is called *the steer equation*. Written in matrix form we have [1]:

$$\mathbf{M}\ddot{\mathbf{q}} + [v \cdot \mathbf{C_1}]\dot{\mathbf{q}} + [\mathbf{K_0} + v^2 \cdot \mathbf{K_2}]\mathbf{q} = \mathbf{f}, \tag{2}$$

where the time-varying variables are

$$\mathbf{q} = \left[\begin{array}{c} \phi \\ \delta \end{array} \right] \qquad \text{and the forcing} \qquad \mathbf{f} = \left[\begin{array}{c} T_\phi \\ T_\delta \end{array} \right].$$

The constant coefficients of $\ddot{\mathbf{q}}, \dot{\mathbf{q}}$ and $\mathbf{q}$ are presented algorithmically in terms of the bicycle design parameters in [1]. Briefly, they are a symmetric mass matrix, $\mathbf{M}$, a "damping" matrix $v\mathbf{C_1}$ which is linear in the forward speed, and a stiffness matrix which is the sum of a constant (symmetric) part, $\mathbf{K_0}$, and a part, $v^2\mathbf{K_2}$, which is quadratic in the forward speed. For the measured parameters of the instrumented bicycle from table 1 these matrices take on the values:

$$\mathbf{M} = \left[\begin{array}{cc} 7.989\,81, & 0.895\,69 \\ 0.895\,69, & 0.298\,57 \end{array} \right], \quad \mathbf{C1} = \left[\begin{array}{cc} 0, & 7.170\,25 \\ -0.593\,89, & 1.326\,10 \end{array} \right],$$

$$\mathbf{K0} = \left[\begin{array}{cc} -109.911\,68, & -13.457\,45 \\ -13.457\,45, & -4.822\,72 \end{array} \right], \quad \mathbf{K2} = \left[\begin{array}{cc} 0, & 11.197\,98 \\ 0, & 1.422\,00 \end{array} \right]. \tag{3}$$

The transient response of the system, in the absence of any forcing, is given by a linear combination of the eigenmodes. These eigenmodes together with their eigenvalues are found by assuming an exponential solution of the form $\mathbf{q} = \mathbf{q}_0 \exp(\lambda t)$ for the homogeneous equations from (2). This leads to a characteristic polynomial which is quartic in λ. The coefficients in this polynomial are complex expressions of the 25 design parameters, gravity, and speed v. The solutions λ of the characteristic polynomial for a range of forward speeds are shown in figure 3. Eigenvalues with a positive real part correspond to unstable motions whereas eigenvalues with
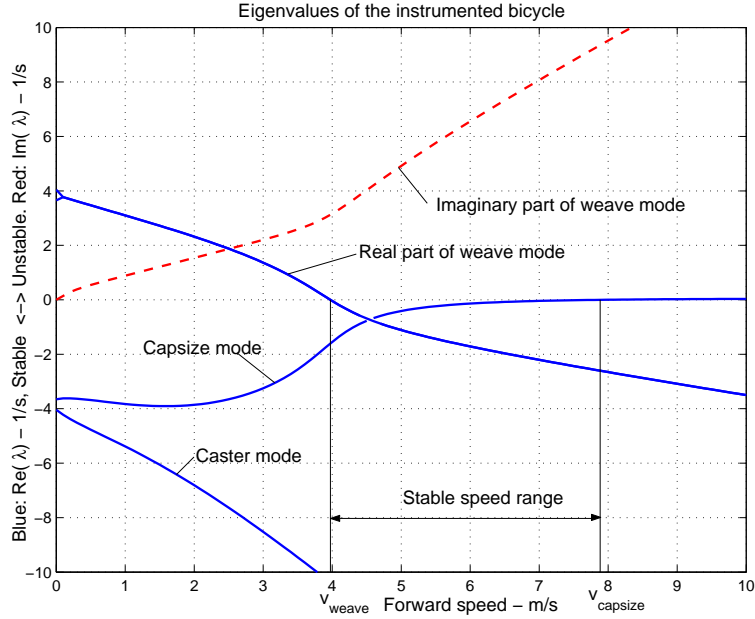
4

Figure 3: The eigenvalues for the instrumented bicycle as calculated by the linearized model.

a negative real part correspond to asymptotically stable motions for the corresponding mode. Imaginary eigenvalues correspond to oscillatory motions.

In principle there are up to four eigenmodes, where oscillatory eigenmodes come in pairs. Two are significant and are traditionally called the *capsize mode* and *weave mode*. The capsize mode corresponds to a real eigenvalue with eigenvector dominated by lean: when unstable, the bicycle just falls over like a capsizing ship. The weave mode is an oscillatory motion in which the bicycle sways about the headed direction. The third remaining eigenmode is the *caster mode* which corresponds to a large negative real eigenvalue with eigenvector dominated by steering.

At very low speeds, typically $0 < v < 0.1$ m/s, there are two positive and two negative eigenvalues which correspond to an inverted-pendulum-like motion of the bicycle. Then at $v \approx 0.067$ m/s two real eigenvalues become identical and form a complex conjugate pair; this is where the oscillatory weave motion emerges. At first this motion is unstable but at $v_{weave} \approx 3.986$ m/s, the weave speed, these eigenvalues cross the real axis in a Hopf bifurcation and the weave motion becomes stable up to infinite speed. At high speeds the frequency of the weave motion is approximately proportional to the forward speed, meaning that the wavelength of the oscillation becomes constant. Meanwhile the capsize motion, which was stable for low speed, crosses the real axis in a pitchfork bifurcation at $v_{capsize} \approx 7.896$ m/s, the capsize speed, and the motion becomes mildly unstable. With further increase in speed, the unstable capsize eigenvalue approaches zero (from above). The speed range for which the uncontrolled bicycle shows asymptotically stable behaviour is $v_{weave} < v < v_{capsize}$.

From this analysis we conclude that the principal motion of the bicycle to be expected during measurement is the oscillatory weave motion. The frequency of this motion is low, less than 1 Hz and the breakpoint between unstable and stable motion is around 4 m/s. This is a speed which can easily be reached by manual launching. The caster mode is highly damped and will disappear quickly from the transient response. The same can be said for the stable capsize mode for forward speeds up to 3 m/s. The maximum attainable forward speed for manual launching is around 6 m/s and therefore the mildly unstable capsize mode will never be encountered.
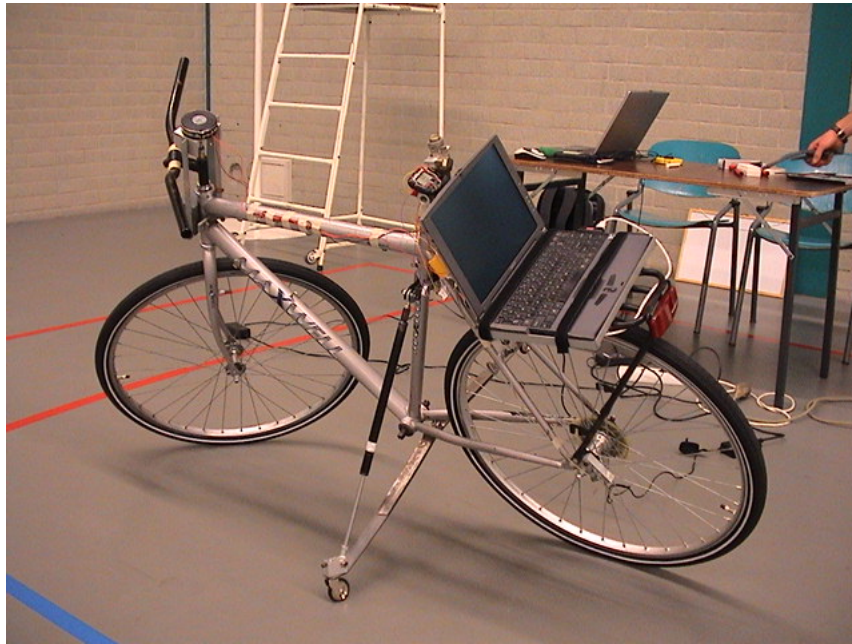
5

Figure 4: The instrumented bicycle with all the measurement equipment installed.

3 INSTRUMENTED BICYCLE

The experimental system consists of an instrumented bicycle without rider. Sensors are present for measuring the roll rate and the yaw rate, the steering angle and the rear wheel rotation. The data are collected on a laptop computer mounted on the rear rack. Trainer wheels prevent the complete fall of the bicycle for unstable conditions. Measurements are recorded for the case in which the bicycle coasts freely on a level surface.

3.1 The Bicycle

The instrumented bicycle used in the tests was a typical 21" city-bicycle with 28" wheels, brand 'Maxwell', type 'Silvercity', see figure 4. For the experiments all the superfluous parts on the bicycle were removed. What remained was the rear frame with bottom bracket and the rear rack, the front fork and the handlebar, front wheel and the rear wheel with sprocket-wheel cassette.

Side wheels were added to the bicycle to reduce the maximum lean angle by which the bicycle could tip over to approx $30°$. The sidewheels were connected via a suspension construction consisting of two metal strips acting as a spring and two telescopic dampers, which had the air removed, to act as a guide. The front fork was flipped (rotated by $180°$) to increase the trail. This lowers the weave speed and by such increases the stable speed range. In this way we were able to make better use of the limited space available for the tests. The head tube bearings and the wheel hub bearings were cleaned and reinstalled to reduce play and excessive friction. New tires, standard $28 \times 1\frac{3}{8}$ brand 'Halfords', and new inner tubes were mounted. The tires were inflated to 3.5 bar overpressure. The rims were checked for trueness. No rim wobble was noted.

3.2 Measuring Equipment Requirements

The following requirements were assigned to the measuring equipment:

- The only effect on the dynamic behaviour was that of added weight and inertia.

- No extra degrees of freedom allowed by non-rigidly attaching parts.

- To be used on most standard bicycles with little adjustments.

- Withstand moderate shocks.

- Low budget, $< \$ 1500$.

3.3 Measuring equipment

The following equipment was used:

Laptop: For data collection a laptop was used, brand ACER 340 Travelmate with a Sitecom USB 2.0 PCMCIA card installed. The laptop was placed on the rear carrier which reduced the dynamic stability of the bicycle [5] but the fixation was easily achieved whilst remaining compatible for other bicycles. The laptop was placed in a steel frame with padding that was mechanically bolted to the rear carrier such that the centre of mass of the laptop and steel frame was over the bicycle symmetry plane. The laptop was kept in the frame by two Velcro straps.

Steering angle sensor: A potentiometer, brand Duncan Electronics Inc. 1801 Single turn, 358 degree was used with the following specifications: Resistance: 20K $\pm 3\%$ Ohm and Linearity: $\pm 0.75\%$. Most "standard" Dutch bicycles have a head tube with an outer diameter of 34 mm. Therefore a bracket with two vertically mounted steel L shaped rods connected to an aluminium U profile kept the potentiometer in position. The rods also restricted the maximum angle that the front frame could make with respect to the rear to about $30°$, reducing the chance that the bicycle could flip over. Minimal play was achieved between the potentiometer and the front frame by directly connecting the sensor to the steering axis via a flexible coupling that compensated for a small misalignment of the steering axis with the sensor axis. A transmission was thus avoided. A drawback to this method was that the output range of the signal was small.

Angular rate sensors: Two angular rate gyros, brand Silicon Sensing CRS03 with a rate range of ± 100 degs/s were used to measure the lean rate and the yaw rate of the rear frame. The two rate sensors were placed perpendicular to each other on a T profile that was clamped to the saddle post. A rotational spirit level was placed on top of the yaw rate sensor to ensure that it was placed horizontally.

Battery pack: The DC power supply for the rate gyros was a battery pack, brand BMI NI-CD 4.8V 2100mAh, cable tied to the rear frame.

Data acquisition unit: A USB connected data acquisition unit brand, National Instruments NI-USB-6009, was used. This unit has eight 14-bit analogue input channels, 12 digital I/O lines, 2 analogue outputs and 1 counter. Only the analogue inputs were used. The data acquisition unit was bolted to the rear carrier.

Forward speed sensor: Forward speed was measured by means of a standard speedometer, brand Avocet Altimeter 50. This unit uses a a magnetic ring with 10 north/south poles and a pickup. The pickup was connected to one of the analogue channels of the USB data acquisition unit.

The forward speed of the bicycle was previously defined as the rear wheel rotation speed multiplied by the effective tire radius, thus the ring was glued to the rear wheel.

The bicycle computer was placed on an aluminium shaft that was connected to the saddle clamp. With the bicycle computer in this position the speed values shown on its screen were clearly legible when running behind and alongside the bicycle. However, the refresh rate of the computer was too slow and full attention of the launcher was usually needed to launch the bicycle in a proper manner.

4 MEASURING BICYCLE DESIGN PARAMETERS

Table 1 shows the measured values for all twenty five design parameters for the instrumented bicycle. The bicycle was measured with all the measurement equipment installed, including the laptop and sidewheels. The twenty five parameters can be divided into two groups, geometrical properties and mass properties.

4.1 Geometrical properties

The following geometrical parameters shown schematically in figure 2 were measured.

Wheelbase: The distance from the centre of the front contact patch to the centre of the rear contact patch measured on level ground whilst the front fork was aligned with the rear frame.

Head angle: Measured on level ground with the bicycle vertical by placing a protractor with integrated spirit level against the front of the head tube.

Trail: On level ground with the bicycle vertical and with the front fork facing forwards. By extending the head tube by means of a plate and rod such that the point of intersection with the level ground was located. The trail was then measured by measuring the distance parallel to the x-axis of the bicycle between the contact point of the front wheel and the intersection of the head tube with the ground.

Wheel radius: Was calculated by measuring the distance covered by the bicycle, when the wheel that was being measured, travelled nine full rotations along a straight line on a level floor, where the tires were inflated to 3.5 bar overpressure. Nine rotations were used as this was the maximum amount that could be measured with a 30 m long measuring tape. The measured distance was then divided by 18π to get the effective rolling radius.

4.2 Mass properties

The mathematical model requires the mass and inertia properties of the four separate parts: rear wheel, rear frame assembly, front handlebar assembly and front wheel. For each part the mass, the location of its centre of gravity and the mass moments of inertia with respect to axis through the centre of mass and parallel to the global xyz-axes in the reference position (see figure 2) had to be found.

The mass of the parts was easily measured on a set of scales to an accuracy of ± 0.01 kg. Determining the mass moments of inertia of the parts turned out to be more difficult.

Given the simple geometry of the four bicycle parts one would think it would be easy to calculate the mass moment of inertia from a measured geometry model. However, four serious problems were encountered:

1. All the measuring equipment, their brackets and the sidewheel construction had to be modelled. Since none of the sensors or the computer have constant densities, assigning the correct mass moments of inertia to them without actually measuring them is virtually impossible.

2. The wall thickness of most of the tubes was not known. Thus without drilling a hole in most of the tubes these could not be measured. It was also unknown if the wall thickness was constant in each tube.

3. Most of the tubes of the front and rear frame do not have a constant cross-section, increasing the complexity of the model.

Thus it was decided that the mass moments of inertia parameters of the instrumented bicycle would be measured instead. A torsion pendulum was constructed to this end.

4.2.1 Measuring the mass moments of inertia

The mass moments of inertia of the four individual parts were measured by means of a torsional pendulum, see figure 5. The torsional pendulum was made of a 1 m long, 5 mm diameter slender steel rod that was clamped vertically at the upper end. The lower end of the rod was connected by a stiff coupling to the bicycle part that was to be measured. The torsion rod was clamped over 4 cm of its length at both ends leaving 92 cm free length.

The bicycle part was manually set into an angular oscillation and the time period of the oscillation was measured. The part was only given small rotations to ensure elastic material behaviour in the rod.

The bicycle part was clamped such that its center of gravity was aligned with the rotational axis of the rod. This ensured that measurement was made about a centre of mass axis of the part and that there was no bending moment in the rod that could disturb the angular oscillation of the system.

The equation of motion for the torsion pendulum is given by

$$I_M \ddot{\theta} + \left[\frac{GI_P}{L} \right] \theta = 0 \tag{4}$$

Where, I_M is the mass moment of inertia of the bicycle and pendulum construction, $\ddot{\theta}$ the angular acceleration of the lower end of the rod, L is the length of the rod, G the shear modulus of elasticity of the rod material (steel) and I_P the polar moment of inertia of the rod. The moment of inertia of the clamp that held the bicycle part was very small compared to that of the bicycle part, and its contribution was neglected. Therefore the moment of inertia of the to be measured part along the rod axis could be calculated as

$$I_M = \left(\frac{T}{2\pi} \right)^2 \left[\frac{GI_P}{L} \right], \tag{5}$$

where T is the time period for one oscillation.

Figure 5: The rear frame clamped in the torsional pendulum.

Under the assumption that all parts have a vertical symmetry plane only four out of the in general six mass moment of inertia terms of the 3 by 3 inertia matrix had to determined. Moreover, since the pitch motion is not present in the linearized model of the upright bicycle there was no need to measure the mass moment of inertia along this pitch axis (I_{yy}), an educated guess was made. This reduced the number of measurements to three.

The experiment was carried out on the three main frame tubes of the rear frame: the sloping lower tube, the top tube and the seat tube. For the front frame the experiment was carried out with the clamp on the head tube about the pitch and roll axes and about the handlebar for the yaw axis. Figure 5 shows the rear frame, with the saddle tube held in the clamp.

4.3   Processing of the mass moments of inertia

In order to be able to calculate the mass moments of inertia in the global axes about the centre of mass for the different parts, the moment of inertia tensors had to be rotated. To do this the angle under which the frame had been hung had to be calculated. Photographs were taken, with the camera held horizontally, perpendicular to the frame, with each photograph taken in the same position and the same distance from the part for each of the experiments. Then together with the information that the top tube has a $5°$ slope relative to the global x-axis when the bicycle is on level ground, the angle under which the frame was hung in each case relative to the global x-axis was calculated.

Next the position of the centre of mass was found. Using the same photographs and placing them on top of one another and extending the torsion rods the location of the centre of mass was found. The location of the centre of mass of the part as found in the photograph was then transformed to the global coordinates by measuring tube lengths in the photographs, comparing them with the actual lengths and calculating the scale factor.

In order to measure the entries in the mass moment of inertia matrix for the xz-plane, which is the plane of symmetry, three measurements along different axis had to be made. By noting that:

$$\begin{aligned} \mathbf{M} &= \mathbf{I}\dot{\boldsymbol{\omega}} + \boldsymbol{\omega} \times (\mathbf{I}\boldsymbol{\omega}) \,, \text{where} \\ \boldsymbol{\omega} &= \dot{\varphi}\mathbf{e}_i \end{aligned} \tag{6}$$

$$
\begin{aligned}
\dot{\boldsymbol{\omega}} &= \ddot{\varphi}\mathbf{e}_i \text{ , and where} \\
\mathbf{e}_i &= \quad \text{is the unit vector rotation axis. Therefore :} \\
\mathbf{e}_i^T \mathbf{M} &= \mathbf{e}_i^T \left(\mathbf{I}\ddot{\varphi}\mathbf{e}_i + \dot{\varphi}\mathbf{e}_i \times (\mathbf{I}\dot{\varphi}\mathbf{e}_i) \right) &\text{(7)} \\
M_i &= \mathbf{e}_i^T \mathbf{I}\mathbf{e}_i \ddot{\varphi} \text{ , where} &\text{(8)}
\end{aligned}
$$

$$
\mathbf{e}_i^T \mathbf{I}\mathbf{e}_i =
\begin{bmatrix} e_{x_i} \\ 0 \\ e_{z_i} \end{bmatrix}^T
\begin{bmatrix} I_{xx} & I_{xy} & I_{xz} \\ I_{xy} & I_{yy} & I_{yz} \\ I_{xz} & I_{yz} & I_{zz} \end{bmatrix}
\begin{bmatrix} e_{x_i} \\ 0 \\ e_{z_i} \end{bmatrix}
\tag{9}
$$

Thus the measured mass moment of inertia I_i along the $\mathbf{e}_i$ axis is

$$
e_{x_i} I_{xx} e_{x_i} + 2 e_{x_i} I_{xz} e_{z_i} + e_{z_i} I_{zz} e_{z_i} = I_i \text{ , for i} = 1, 2, 3.
\tag{10}
$$

Where 1,2,3 are the three different axis about which the moment of inertia was measured. By solving the following matrix equation,

$$
\begin{bmatrix} e_{x_1}^2 & 2e_{x_1}e_{z_1} & e_{z_1}^2 \\ e_{x_2}^2 & 2e_{x_2}e_{z_2} & e_{z_2}^2 \\ e_{x_3}^2 & 2e_{x_3}e_{z_3} & e_{z_3}^2 \end{bmatrix}
\begin{bmatrix} I_{xx} \\ I_{xz} \\ I_{zz} \end{bmatrix}
=
\begin{bmatrix} I_1 \\ I_2 \\ I_3 \end{bmatrix}
\tag{11}
$$

the components of the mass moments of inertia with respect to the global reference from I_{xx}, I_{xz} and I_{zz} were found.

With the xz-plane of the bicycle being the plane of symmetry, the off diagonal terms I_{xy} and I_{yz} are both zero. The frame is not exactly symmetrical due to the small welded parts that are used to attach accessories, such as the dynamo, to the frame, but these were ignored as they have an insignificant contribution. The front fork and handlebar assembly was measured in the same manner, were it should be noted that the mass moment of inertia about the steering axis was small in comparison with the other entries in the inertia matrix and should have been measured with a more compliant torsion bar.

The wheels were weighed as one complete unit even though in the linearized dynamic model the wheels are modelled as only the rotating part of the wheel. The inaccuracy for the model was considered negligible because the mass of the non rotating parts are located at the centre of the wheel and thus have little contribution towards the moment of inertia about the axle. The axle also weighs relatively little compared with the mass of the rear frame.

The measurement of the wheel inertia was done in two separate tests. The first was carried out using the torsion pendulum described above to measure the inertia about the wheel's global x- and z-axis (identical). The second test was to determine the mass moment of inertia about the axle axis (I_{yy}). In a compound pendulum experiment the wheel was hung from a horizontally placed nail and given a small offset to bring the wheel into an oscillation and the time was measured. Then with the known mass and distance to the centre of mass, the mass moment of inertia about the axle axis could be calculated by application of the parallel axes theorem.

The measured mass moments of inertia and centres of gravity of all parts are presented in table 1.

5 EXPERIMENTAL PROCEDURE AND RESULTS

5.1 Test procedure

To test the assumption that the rolling contact of the bicycle wheels are ideal with no slip experiments were carried out in the university sports hall. The 42×25 m sports hall had a dry, level floor with a rubbery surface layer as can be found in any sports hall.

Parameter	Symbol	Value
Wheel base	w	1.010 m
Trail	t	0.190 m
Head angle	α	69 °
Gravity	g	9.81 N/kg
Forward speed	v	$variable$ m/s
Rear wheel		
Radius	R_{rw}	0.3500 m
Mass	m_{rw}	2.56 kg
Mass moment of inertia	(A_{xx}, A_{yy}, A_{zz})	(0.078, 0.156, 0.078) kgm^2
Rear frame		
Position of centre of mass	(x_{rf}, y_{rf}, z_{rf})	(0.320, 0, -0.627) m
Mass	m_{rf}	12.06 kg
Mass moment of inertia	$\begin{bmatrix} B_{xx} & 0 & B_{xz} \\ 0 & B_{yy} & 0 \\ B_{xz} & 0 & B_{zz} \end{bmatrix}$	$\begin{bmatrix} 0.8155 & 0 & 0.0327 \\ 0 & 1.2 & 0 \\ 0.0327 & 0 & 1.0825 \end{bmatrix}$ kgm^2
Front frame		
Position of centre of mass	(x_{ff}, y_{ff}, z_{ff})	(0.907, 0, -0.800) m
Mass	m_{ff}	2.54 kg
Mass moment of inertia	$\begin{bmatrix} C_{xx} & 0 & C_{xz} \\ 0 & C_{yy} & 0 \\ C_{xz} & 0 & C_{zz} \end{bmatrix}$	$\begin{bmatrix} 0.0860 & 0 & -0.0311 \\ 0 & 0.1 & 0 \\ -0.0311 & 0 & 0.0169 \end{bmatrix}$ kgm^2
Front wheel		
Radius	R_{fw}	0.3485 m
Mass	m_{fw}	2.05 kg
Mass moment of inertia	(D_{xx}, D_{yy}, D_{zz})	(0.081, 0.162, 0.081) kgm^2

Table 1: The measured design parameters for the instrumented bicycle from figure 2 and 4.

In total 76 runs were carried out. Each run consisted of three segments. In the first segment the bicycle was brought up to speed and during high speed runs the bicycle was then laterally perturbed. In the second segment the bicycle was allowed to coast freely and in third segment the bicycle was brought back to standstill.

A restriction on the spread of the measurements was the top speed of the person propelling the bicycle along as the person not only had to be able to accelerate the bicycle in as short a distance as possible but also had to be able run alongside the bicycle and bring it back to a standstill before it collided with the wall.

To measure the dynamic response of the bicycle at the different speeds and calculate the corresponding motion eigenvalues the bicycle had to show some lateral dynamics. At speeds below the stable speed range no external excitation was required. Due to small asymmetry or non perfect initial conditions the bicycle always started to weave about its general heading and this motion was measured. Moreover, the small asymmetry caused the bicycle to lean to the right when released, which thereby ended up rolling in a large circle rather than a straight line.

For runs in the stable speed range the bicycle set itself in an upright position and showed no dynamic behaviour unless it was given a lateral excitation. This excitation was accomplished by applying a lateral impulse to the bicycle by simply hitting the bicycle's rear frame by hand in the lateral direction.

Two runs were carried out whilst stationary to determine the zero speed inverted pendulum eigenvalue, eight runs were carried out at low speed (around 2 m/s), the majority of the tests (56) were carried out in the transition region from unstable weave to stable weave motion (3.5 - 5 m/s) and ten tests were carried out at higher speeds up to about 6 m/s. At forward speed less than 2 m/s the bicycle was very unstable giving only a very short time window to measure.

5.2   Stored Data

The frequency of the weave of motion is low, in the order of 1 Hz and therefore only a low sample rate is needed here. However, the measurement of the forward speed by means of the 10 magnet ring needed a higher sampling rate. The first tests were measured with a 100 Hz sample frequency. Then to ensure no aliasing in the speed signal would take place when testing at a higher speed 400Hz was used. Unfortuantely higher sampling frequencies gave a very erratic signal at the recorder steering angle potentiometer signal. The recorded data for each run was stored in a text file.

Every run was recorder on video, an example of such a video can be found at [17]. This turned out to be essential for the processing of the run data and helped to identify nonstandard measurements, the quality of the launch, etc. It was thus possible to compare the recorded data afterwards with the video images and extract the relevant data for the calculation of the eigenvalues from each file.

5.3   Data analysis

For each run the raw data was transferred to Matlab and at first inspected visually. A plot of the raw data for run 52 is shown in figure 6. In the figure the battery voltage can be seen (the blue line), the steering angle (magenta), the lean rate (red), the yaw rate (green) and the speed signal (cyan). These graphs were used, together with the videos of the runs, to locate the time
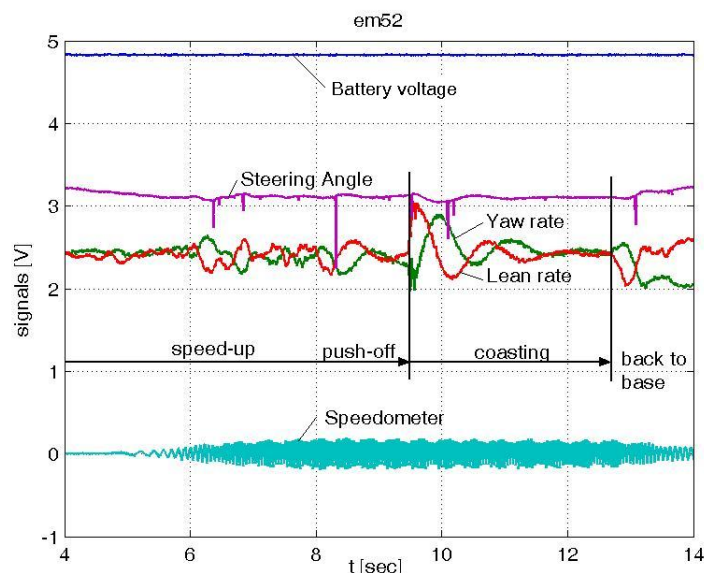

Figure 6: The raw data from run 52, this is around a forward speed of 5 m/s which is clearly within the stable speed range. The signals are: battery voltage (the blue line), steering angle (magenta), lean rate (red), the yaw rate (green) and the forward speed signal (cyan). Note the three different regimes: speed up, coasting, back to base.

window in which the bicycle coasted freely for each run. Once manually located a non-linear

fit of the eigenmotions was preformed on the the lean rate data using Matlab's `fminsearch` to extract the measured eigenvalues, see figure 7. Above a forward speed of 0.1 m/s there is
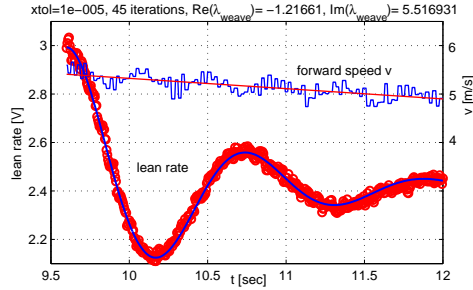

Figure 7: Nonlinear fit of the oscillatory stable lean rate (solid blue line) to the measured data (red circles) and measured eigenvalues for measurement number 52, together with the measured forward speed (ragged blue line). Note the slight decrease in forward speed during the measurement.

in principle a sum of three eigenmodes to be fitted: the caster mode, the capsize mode and the oscillatory weave mode, see figure 3. The caster mode is highly damped and will vanish quickly from the transient signal. The capsize mode is also reasonably damped below the weave speed and is mildly unstable above the weave speed resulting here in a small and slow lean rate offset. Therefore only an exponentially damped or growing oscillatory weave motion was fitted to the data. The fit function for the lean rate was taken as

$$\dot{\phi} = c_1 + e^{dt}[c_2 \cos(\omega t) + c_3 \sin(\omega t)], \tag{12}$$

with the weave frequency $\omega = \text{Im}(\lambda_{weave})$, the weave damping $d = \text{Re}(\lambda_{weave})$ and the three constants: c_1 for the offset, c_2 for the cosine amplitude and c_3 for the sine amplitude.

The speedometer signal, see figure 6, was an oscillatory signal with a frequency of ten times the rear wheel rotation frequency. The signal was converted to a forward speed by counting the time between each each zero crossing. As each crossing represents a $1/20$th of a complete rear wheel rotation an average speed for that portion could be calculated; this is the blue ragged line in figure 7. As the forward speed during the coasting section of the measurements slowly decreased due to air resistance, and rolling resistance one speed range was assigned to the calculated λ's instead of a specific speed. This speed range was calculated by looking at a linear fit of the speed for the chosen window, see figure 7. Finally, in figure 8, the measured eigenvalues were plotted on top of the calculated eigenvalues for all runs where horizontal bars are used to indicated the forward speed variation during the measurements.

At zero speed two measurement were made (number 40 and 41). Since the bicycle just falls over in an inverted pendulum manner only an exponential growing solution was fitted to the lean rate data and only one eigenvalue was extracted.

5.4 Discussion

In the unstable speed region below 3 m/s it turned out to be very difficult to measure the motion of the bicycle. The time window for measurement was very short at these speeds making fitting a harmonic function to the measured data very difficult.

At speeds above 3 m/s the predicted weave frequency and damping by the model were forecasted accurately. The transition from the unstable to the stable region around the weave speed is accurately described by the model.
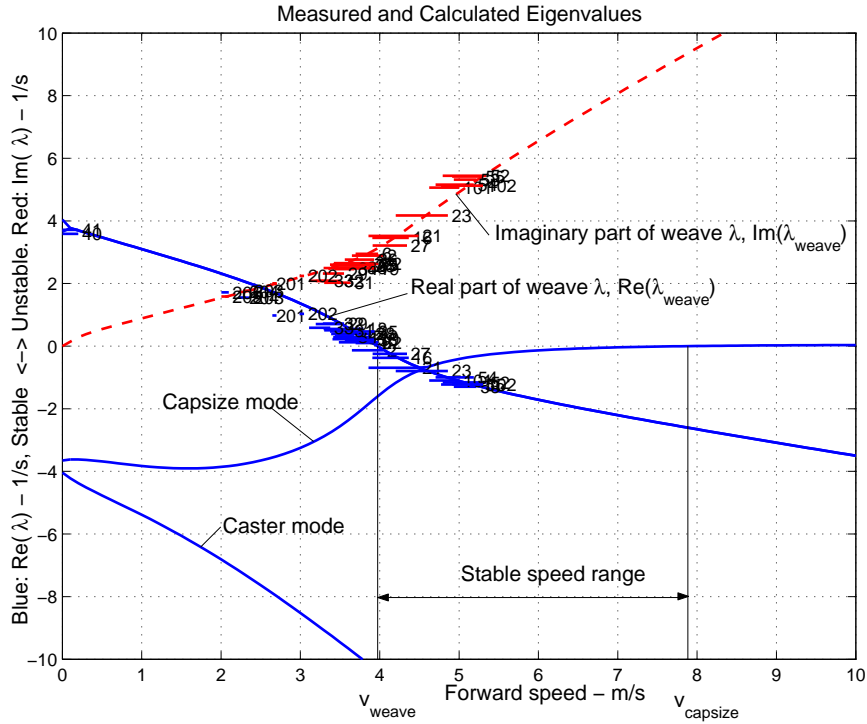
Figure 8: Measured (horizontal stripes) and calculated (continuous lines) eigenvalues for the instrumented bicycle. For the measurements only the weave motion is considered. The length of the horizontal stripes indicate the forward speed range during the measurement, numbers indicate the corresponding test run.

At speeds greater than approximately 5 m/s the weave-frequency that was extracted from the data is slightly higher than that of the model. This difference can be explained by the weighing of the linearized speed towards the end of the measurement window speeds as initially during the run the larger air resistance caused by the, vertically placed, laptop screen caused the bicycle to slow down far more rapidly than at the end of the window. Therefore when the measured speed was linearized the initial (highest) speed was underestimated and thus the eigenfrequency that was found was recorded for a lower speed than that actually occurred during the measurement.

The yaw rate signal was of the same quality as the lean rate signal. The steering rate signal turned out to be too small and too erratic to use.

In retrospect mounting slick racing tires with a low rolling resistance and at a high pressure (around 8 bar) would have reduced the rolling resistance and thus reduced the speed range for the calculated eigenvalues.

6 CONCLUSIONS

The experimental results show a very good agreement with the results as obtained by a linearized analysis on a dynamic model of an uncontrolled bicycle. This shows that the tire slip and frame and fork compliance are not important for the lateral dynamics of the bicycle in the speed range up to 6 m/s. The validated model can be used to design a controller for the unstable bicycle.

REFERENCES

[1] A. L. Schwab, J. P. Meijaard, and J. M. Papadopoulos, A Multibody Dynamics Benchmark on the Equations of Motion of an Uncontrolled Bicycle. In *Proceedings of the Fifth EU-ROMECH Nonlinear Dynamics Conference, ENOC-2005, August 7–12, 2005, Eindhoven University of Technology, The Netherlands*, 511–521, 2005.

[2] E. Döhring, Über die Stabilität und die Lenkkräfte von Einspurfahrzeugen. Ph.D. thesis, Technical University Braunschweig, Germany, 1953.

[3] E. Döhring, Die Stabilität von Einspurfahrzeugen. *Automobil Technische Zeitschrift*, **56**(3), 68–72, 1954.

[4] R. S. Rice and R. D. Roland, An evaluation of the performance and handling qualities of bicycles. Cornell Aero. Lab. Report no. VJ-2888-K, 1970.

[5] R. D. Roland and J. P. Lynch, Bicycle dynamics tire characteristics and rider modeling. Cornell Aero. Lab. Report no. YA-3063-K-2, 1972.

[6] R. D. Roland and D. E. Massing, A digital computer simulation of bicycle dynamics. Cornell Aero. Lab. Report no. YA-3063-K-1, 1971.

[7] M. Wächter, Eine experimentelle Überprüfung des dynamischen Fahrradmodells. M.Sc. thesis, University of Oldenburg, Germany, 1991.

[8] W. Suhr, Entwicklung und Erprobung eines nichtlinearen dynamischen Fahrradmodells, excerpts from a Ph.D. thesis, University of Oldenburg, Germany, 1992.

[9] A. W. Jackson and M. Dragovan, An experimental investigation of bicycle dynamics. *American Journal of Physics*, (submitted) 1998.

[10] D. J. Eaton, Man-machine dynamics in the stabilization of single-track vehicles. Ph.D. thesis, University of Michigan, 1973.

[11] R. S. Rice, Accident avoidance capabilities of motorcycles. In *Proceedings International Motorcycle Safety Conference, Dec 16 & 17 , 1975*, USDOT, National Highway Traffic Safety Administration, Washington, DC, 121–134, 1975.

[12] D. H. Weir and J. W. Zellner, Lateral-directional motorcycle dynamics and rider control. Technical report no. 780304, Society of Automotive Engineers, Warrendale, PA, 1978.

[13] P. A. J. Ruijs and H. B. Pacejka, Recent research research in lateral dynamics of motorcycles. In *Proceedings of the 9th IAVSD Symposium held at Linköping University, Linköping, Sweden, June 24–28, 1985*, 467–480, 1986.

[14] S. Miyagishi, I. Kageyama, K. Takama, M. Baba and H. Uchiyama, Study on construction of a rider robot for two-wheeled vehicle, *JSAE Review*, **24**(3), 321–326, 2003

[15] Blue Team, http://www.roboticinfantry.com/

[16] Cossalter, V., *et al.*, http://www.dinamoto.it/

[17] http://tam.cornell.edu/∼als93/bicycledyn.htm#May24